Laboratory Investigation (2020) 100:682–695
https://doi.org/10.1038/s41374-019-0359-x

ARTICLE

S100A4/non-muscle myosin II signaling regulates epithelial-mesenchymal transition and stemness in uterine carcinosarcoma

Masataka Tochimoto[1] · Yasuko Oguri[1] · Miki Hashimura[1] · Ryo Konno[2] · Toshihide Matsumoto[1] · Ako Yokoi[1] · Yoshio Kodera[2] · Makoto Saegusa[1]

Received: 17 September 2019 / Revised: 5 November 2019 / Accepted: 9 November 2019 / Published online: 19 December 2019
© The Author(s), under exclusive licence to United States and Canadian Academy of Pathology 2019

Abstract

Uterine carcinosarcoma (UCS) represents a true example of cancer associated with epithelial-mesenchymal transition (EMT), which exhibits cancer stem cell (CSC)-like traits. Although S100A4 is an inducer of EMT, little is known about its involvement in UCS tumorigenesis. Herein, we focused on the functional role of S100A4 during development of UCS. Expression of S100A4 and molecules associated with its function were also examined in 35 UCS cases. In endometrial carcinoma cell lines, *S100A4* promoter activity and mRNA levels were significantly increased by the transfection of NF-κB/p65, independent of a putative κB-binding site in the promoter. Cells stably overexpressing S100A4 showed enhancement of CSC properties, along with decreased cell proliferation and acceleration of cell migration. These phenotypes were abrogated in S100A4-knockdown cells. A combination of S100A4 antibody-mediated co-immunoprecipitation and shotgun proteomics analysis revealed that S100A4 strongly interacted with non-muscle myosin II (NMII) heavy chains, including myosin 9 and myosin 14. Specific inhibition of NMII by blebbistatin phenocopied S100A4 overexpression and induced a fibroblast-like morphology. In clinical samples, S100A4 score was significantly higher in sarcomatous as compared with carcinomatous components of UCS, and was positively correlated with ALDH1, Slug, and vimentin scores, and inversely with Ki-67 labeling indices. These findings suggest that an S100A4/NMII-related signaling cascade may contribute to the establishment and maintenance of EMT/CSC properties, along with changes in cell proliferation and migration capability. These events may be initiated in carcinomatous components in UCS and lead to divergent sarcomatous differentiation.

Introduction

Uterine carcinosarcomas (UCS) are highly aggressive neoplasms with a biphasic histological appearance featuring both carcinomatous and sarcomatous components [1, 2]. The most common carcinomatous components are serous, followed by endometrioid type, while the sarcomatous elements are subdivided into two subcategories: homologous containing tissues normally found in the uterus and heterologous with non-normal components [1, 3]. Recent studies revealed that most, but not all, UCS are monoclonal, suggesting a common origin for both carcinomatous and sarcomatous elements [4].

Epithelial-mesenchymal transition (EMT), which allows epithelial cells to acquire a mesenchymal phenotype, plays a central role in inducing tumor invasion and metastasis [5]. A hallmark of EMT is lost E-cadherin expression through Snail, Slug, Twist, and ZEB1, which are all repressors of the *E-cadherin* genes [6–10]. Although evidence of full EMT in human malignancies is very rare, breast carcinosarcomas are now considered to represent a true example of complete EMT [11, 12]. In addition, an association between transcriptional repressors of E-cadherin and microRNA is closely linked to EMT activation and maintenance of cell stemness in UCS [13].

A growing body of evidence demonstrates that a very small subpopulation of cancer stem cells (CSCs) or tumor-initiating cells is observed in tumors [14]. CSCs, similar

Supplementary information The online version of this article (https://doi.org/10.1038/s41374-019-0359-x) contains supplementary material, which is available to authorized users.

✉ Makoto Saegusa
msaegusa@med.kitasato-u.ac.jp

[1] Department of Pathology, Kitasato University School of Medicine, Sagamihara, Kanagawa 252-0374, Japan

[2] Center for Disease Proteomics, School of Science, Kitasato University, Sagamihara, Kanagawa 252-0374, Japan

to normal stem cells, are defined as tumor cells that retain the capacity to self-renew and to differentiate into the heterogeneous lineages of cancer cells that comprise tumors [15]. EMT also promotes stem cell properties and further generates cells with CSC-like features [15]. This suggests the presence of sarcomatous stem-like cells that were derived from carcinoma cells; such stem-like cells may act as progenitors for divergent sarcomatous differentiation in UCS.

S100A4 belongs to the S100 family of Ca^{2+}-binding proteins and possesses no enzymatic activity; instead it exerts its effects by interacting with and modulating the activity of other proteins, such as p53, non-muscle myosin IIA (NMIIA), and Annexin 2 [16–18]. In addition to its reported role as a novel marker and regulator of the glioma stem cell phenotype, S100A4 has recently been implicated as the molecular link that couples the mesenchymal transition and stemness in glioblastoma [19]. We therefore hypothesize that S100A4 may also contribute to UCS genesis through determination of the phenotypic characteristics mediated by EMT/CSC properties. To test this, we investigated the relationship between the expression of S100A4 and other molecules related to S100A4 biological function using endometrial carcinoma (Em Ca) cell lines and clinical UCS samples. To identify interacting partners of S100A4, we applied a combination of S100A4 antibody-mediated co-immunoprecipitation and shotgun proteomics analysis.

Methods

Plasmids and cell lines

Full-length cDNA for human *S100A4* (GenBank accession number NM019554) was amplified by polymerase chain reaction (PCR) and was cloned into pcDNA3.1 vector (Invitrogen, Carlsbad, CA, USA). The human *S100A4* promoter (UCSC genome browser, https://genome.ucsc.edu/) between −1976 and +1012 (where +1 represents the transcription start site) was generated by PCR and was cloned into the pGL-3B vector (Promega, Madison, WT, USA). A series of 5′-truncated promoter constructs and site-directed mutagenesis in a putative κB-binding site at a first intron of the *S100A4* gene were also generated by PCR-based methods. S100A4-specific short hairpin RNA (shRNA) oligonucleotides were designed as described previously [20]. Single-stranded S100A4 oligonucleotides were annealed and then cloned into the *BamH*1-*EcoR*V sites of the RNAi-Ready pSIREN-RetroQ vector (Takara, Shiga, Japan), according to the manufacturer's instructions. The primer sequences for the PCR reaction used in this study are listed in Table 1. CMV-GFP-NMHC II-A (non-muscle, heavy chain, class II, isoform A)(myosin 9, heavy chain; MYH9) was a gift from Dr Robert Adelstein (Addgene plasmid #11347; https://n2t.net/addgene:11347; RRID:Addgene_11347). pcDNA3.1-p65 and pcDNA3.1-Smad2 were used as described previously [20, 21].

Six Em Ca cell lines, Ishikawa and Hec6 cells, as well as Hec50, Hec116, Hec251, and Hec265 cells, were used as described previously [22, 23]. S100A4 expression plasmid or empty vector was transfected into Hec6 cells (which lack endogenous S100A4 expression) and stable over-expressing clones were established. We also established S100A4-knockdown Ishikawa cells (which have relatively high S100A4 expression) using an shRNA targeting the *S100A4* gene (Supplementary Fig. S1), as described previously [20, 21].

Antibodies and reagents

Anti-Rb, anti-N-cadherin, anti-aldehyde dehydrogenase (ALDH)1, anti-nuclear factor (NF)-κB subunit p65 (p65), and anti-$p27^{kip1}$ antibodies were purchased from BD Biosciences (San Jose, CA, USA). Anti-S100A4, anti-Smad2, anti-phospho-Smad2 at Serine 255 (pSmad2), anti-Sox2, anti-Histone H1, anti-phospho-p65 at Serine 536 (pp65), and anti-Twist1 antibodies were obtained from Abcam (Cambridge, MA, USA). Anti-phospho-Serine 807/811 Rb (pRb), anti-vimentin, and anti-Slug antibodies were from Cell Signaling (Danvers, MA, USA). Anti-$p21^{waf1}$, anti-cyclin D1, and anti-p53 antibodies were purchased from Dako (Copenhagen, Denmark). Anti-ZEB1 and anti-β-actin antibodies were obtained from Sigma-Aldrich Chemicals (St. Louis, MO, USA). Anti-cyclin A2, anti-$p16^{INK4A}$, and anti-NMIIA (MYH9) were from Novocastra (Newcastle, UK), SantaCruz Biotechnology (Santa Cruz, CA, USA), and Proteintech (Rosemont, IL, USA), respectively. Anti-E-cadherin, anti-CD133, and anti-NMIIC (myosin 14, heavy chain: MYH14) were from Takara (Shiga, Japan), Miltenyi Biotechnology (Bergisch Gladbach, Germany), and MyBiosource com (San Diego, CA, USA), respectively.

Recombinant tumor necrosis factor (TNF)-α and transforming growth factor (TGF)-β1 were purchased from R&D Systems (Minneapolis, MN, USA). Rapamycin, aphidicolin, and nocodazole for the synchronization of cells at the G1, early S, and G2/M phases, respectively, were obtained from Calbiochem (Cambridge, MA, USA). Blebbistatin was from Toronto Research Chemicals (North York, ON, Canada).

Transfection

Transfection was carried out using LipofectAMINE PLUS (Invitrogen, Carlsbad, CA, USA), and luciferase activity was assayed as described previously [22, 24].

Table 1 Primer sequences for functional analysis of *S100A4* gene used in this study.

Assay	Sequence	
Promoter (−1976/+1012)	Forward	5′-AGGTGGACTTTGTGGAGTATGTGCG-3′
	Reverse	5′-GACAGCAGTCAGGATCTGGGAGCAGGAG-3′
Promoter (−1512/+1012)	Forward	5′-TTGGTTCTTCTCTGAGGACGCGT-3′
	Reverse	5′-GACAGCAGTCAGGATCTGGGAGCAGGAG-3′
Promoter (−1164/+1012)	Forward	5′-GGTGTCTGAGGTGTTTCTCCCA-3′
	Reverse	5′-GACAGCAGTCAGGATCTGGGAGCAGGAG-3′
Promoter (−447/+1012)	Forward	5′-TAGGCTGGTCTTGAACTCCTGGC-3′
	Reverse	5′-GACAGCAGTCAGGATCTGGGAGCAGGAG-3′
Promoter (site-direct mutagenesis)	Forward	5′-GATAGTCTGCtgcccgaatctccagagcttgcg-3′
	Reverse	5′-agggcctcccaggccttgcctcaacaacag-3′
cDNA/mRNA	Forward	5′-GCCACCATGGCGTGCCCTCTGGAGAA-3′
	Reverse	5′-TCATTTCTTCCTGGGCTGCTTATCTG-3′
shRNA (position 69–87)	Forward	5′-gatccgGGGTGACAAGTTCAAGCTCttcaagagaGAGCTTGAACTTGTCACCCtttttg-3′
	Reverse	5′-aattcaaaaaaGGGTGACAAGTTCAAGCTCtctcttgaaGAGCTTGAACTTGTCACCCcg-3′

Reverse transcription PCR (RT-PCR)

cDNA was synthesized from 2 μg of total RNA. Amplification by RT-PCR was carried out in the exponential phase to allow comparison among cDNA synthesized from identical reaction using specific primers (Table 1). Primers for the *GAPDH* gene were also applied, as described previously [22, 24].

Western blot assay and immunoprecipitation

Total cellular proteins were isolated using RIPA buffer [20 mM Tris-HCl (pH 7.2), 1% Nonidet P-40, 0.5% sodium deoxycholate, 0.1% sodium dodecyl sulfate]. Aliquots of the proteins were resolved by SDS-PAGE, transferred to membranes, and probed with primary antibodies, coupled with the ECL detection system (Amersham Pharmacia Biotechnology, Tokyo, Japan).

For immunoprecipitation, cells were lysed with IP buffer [10 mM Tris-HCl (pH 7.6), 100 mM NaCl, 10% NP-40] in the presence of 1 mM $CaCl_2$. Cell lysates were cleared and incubated with anti-S100A4 or anti-NMIIA antibodies, followed by incubation with Protein G-Sepharose (Amersham Pharmacia Biotechnology). Western blot assay was subsequently performed with anti-S100A4 and anti-NMIIA antibodies.

Flow cytometry and Aldefluor assay

Cells were fixed using 70% alcohol and stained with propidium iodide (Sigma) for cell cycle analysis. ALDH1 enzyme activity in viable cells was determined using a fluorogenic dye-based Aldefluor assay (Stem Cell Technologies, Grenoble, France) according to the manufacturer's instructions. The prepared cells were analyzed by flow cytometry using BD FACS Calibur (BD Biosciences) and CellQuest Pro software version 3.3 (BD Biosciences).

Immunofluorescence

After co-transfection of pcDNA3.1-S100A4 and CMV-GFP-NMHC II-A, cells were incubated with anti-S100A4 antibody. Rhodamine-labeled anti-rabbit IgG (Molecular Probes, Eugene, OR, USA) was used as secondary antibody.

Spheroid assay

Cells ($\times 10^3$) were plated in low cell binding plates (Thermo Fisher Scientific, Yokohama, Japan) in serum-free medium. Uniform spheroids of at least 50 μm in diameter were counted ~2 weeks after plating.

Cell Counting Kit-8 assay

The quantitation of viable cell number in proliferation after blebbistatin treatment was carried out using a Cell Counting Kit-8 (CCK-8; Dojindo Lab, Kumamoto, Japan), according to the manufacturer's instructions.

Senescence-associated β-galactosidase (SA-β-gal) and senescence-like cell assay

After treatment with blebbistatin, cells were stained for SA-β-gal activity as described previously [25]. The number of positive cells was analyzed by counting the mean number of SA-β-positive cells per five high-power fields (HPF). Senescence-like cells, which demonstrate more spread and

flattened features, as described previously [25], were also counted in a similar manner.

Wound-healing assay

Cells were seeded equivalently into 24-well tissue culture plates, and grown to reach almost total confluence. After a cell monolayer formed, a wound was scratched with a sterile 200-µl tip. The area of the wound was analyzed using ImageJ software version 1.41 (NIH, Bethesda, MD, USA). Cell migration parameters were calculated in pixels as wound closure.

Migration assay

Cell migration was determined using 24-well transwell chambers with an 8-µm pore size (Corning, NY, USA). The lower chamber was filled with medium containing 10% serum. Cell were suspended in serum-free upper medium with or without blebbistatin and placed into the upper chamber. After 24 h, the number of cells stained by hematoxylin–eosin (HE) on the bottom surface of the polycarbonate membranes was counted visually using a light microscope.

Co-immunoprecipitation and shotgun proteomics analysis

For co-immunoprecipitation, anti-S100A4 antibody was bound and crosslinked to Protein G Dynabeads (Invitrogen) according to the manufacturers' instructions. Cells were lysed with IP buffer with either 1 mM $CaCl_2$ or 1 mM EGTA (or their absence) and the resulting supernatant was incubated with S100A4 antibody-conjugated Protein G Dynabeads in lysate solution. The beads were washed and co-immunoprecipitated materials were then recovered.

Shotgun proteomics using the S100A4-mediated co-immunoprecipitated proteins was then performed. Briefly, samples were alkylated using 55 mM iodoacetamide for 0.5 h and enzymatically digested overnight using trypsin (Promega, Madison, WI, USA) and lysyl endopeptidase (Wako Pure Chemical Industries Ltd, Osaka, Japan). The digested samples were acidified with 0.5% trifluoroacetic acid to precipitate surfactants and were desalted with C18-StageTips, followed by lyophilization. The lyophilized samples were dissolved in 3% acetonitrile and 0.1% formic acid. The peptides were injected into an analytical column: C18 0.075 × 120 mm (Nano HPLC Capillary Column; Nikkyo Technos, Tokyo, Japan), which was attached to an EASY-nLC 1000 liquid chromatograph (Thermo Fisher Scientific). The flow rate of the mobile phases was 300 nL/min, which consisted of (A) 0.1% formic acid, and (B) 0.1% formic acid and 90% acetonitrile. Peptides separated by HPLC with 26 min gradient (5–50% B) were introduced to the Q-Exactive mass spectrometer (Thermo Fisher Scientific).

The Q-Exactive instrument was operated in a data-dependent mode to automatically switch between full-scan MS and MS/MS acquisition. Full-scan MS spectra (m/z 350 −900) were acquired in the Orbitrap with a 70,000 resolution at m/z 200 after the accumulation of ions to a 1×10^6 target value. Tandem mass spectra were acquired in the Orbitrap mass analyzer with a mass resolution of 17,500 at m/z 200 after accumulation of ions to a 2×10^5 target value.

Mass spectral data and database search parameters were processed using a previous method [26, 27]. The quantitative analysis of shotgun proteomics data was achieved by spectral counting. Cluster and volcano plot analyses of the data were conducted by the Ward method using R version 3.3.1 software (R Foundation for Statistical Computing, Vienna, Austria).

TCGA data analysis

The Cancer Genome Atlas (TCGA) UCS annotated gene alteration and mRNA expression data (RNA Seq V2 PSEM) for *S100A4* and *MYH9* genes were extracted from cBioportal for Cancer Genomics (http://www.cbioportal.org/) for 56 UCS cases.

Clinical cases

We reviewed cases of comprehensively staged high-grade endometrial adenocarcinomas from the patient records of Kitasato University Hospital in the period from 1997 to 2018. According to the criteria of the 2014 World Health Organization classification [28], tumors were designated as UCS if they had evidence of both malignant epithelial (endometrioid, serous, or clear cell) components and mesenchymal (homologous or heterologous) elements. Endometrioid adenocarcinomas with spindle elements and hyalinized stroma were specifically excluded. In total, 35 UCS were investigated (Supplementary Table S1). All tissues were routinely fixed in 10% formalin and processed for embedding in paraffin wax. Approval for this study was given by the Ethics Committee of the Kitasato University School of Medicine (B19–144).

Immunohistochemistry (IHC)

IHC was performed using a combination of the microwave-oven heating and polymer immunocomplex (Envision, Dako) methods, as described previously [22, 24]. For the evaluation of IHC findings, scoring of nuclear/cytoplasmic immunoreactivity was performed, on the basis of the percentage of immunopositive cells and the immunointensity,

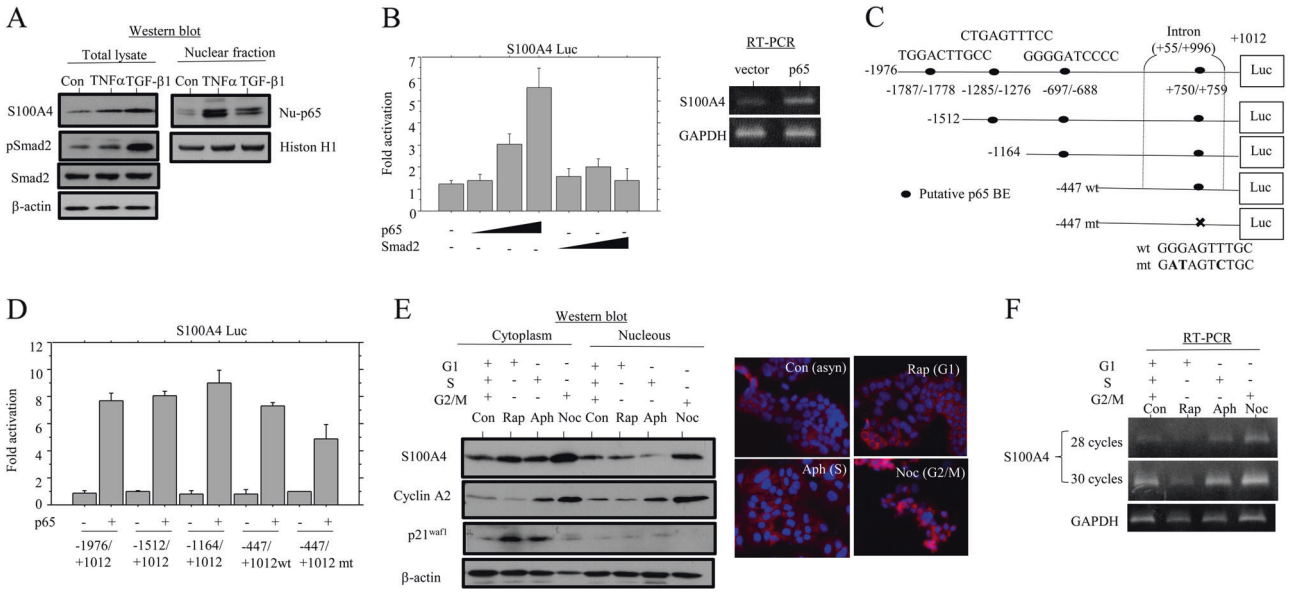

Fig. 1 Regulation of S100A4 expression in Em Ca cells. a Western blot analysis for the indicated proteins in total and nuclear lysates from Ishikawa cells treated with 20 ng/ml TNF-α and 2 ng/ml TGF-β1, respectively. **b** Left: Ishikawa cells were transfected with S100A4 reporter constructs, together with p65 and Smad2, respectively. Relative activity was determined based on arbitrary light units of luciferase activity normalized to pRL-TK activity. The activities of the reporter plus the effector relative to that of the reporter plus empty vector are shown as means ± SDs. The experiment was performed in duplicate. Right: RT-PCR analysis of *S100A4* mRNA levels in total RNA extracted from Ishikawa cells after transfection of p65. **c** The *S100A4* promoter with the first intron sequence containing four putative κB-binding elements (BE). **d** Promoter constructs with various alterations in the first intron were used for evaluating transcriptional regulation of the *S100A4* promoter by p65. The experiment was performed in triplicate. **e** Left: Ishikawa cells were synchronized in the G1 phase by treatment with 50 nM rapamycin, in early S phase by 2 μg/ml aphidicolin, or in the G2/M phase by 0.25 μg/ml nocodazole for 24 h. Western blot assay for proteins in the cytoplasmic and nuclear fractions. Right: after treatment of Ishikawa cells with 50 nM rapamycin, 2 μg/ml aphidicolin, or 0.25 μg/ml nocodazole for 24 h, the cells were stained for S100A4. Note the increased cytoplasmic S100A4 immunoreactivity in the G2/M phase as compared with those of G1 and early S phases. **f** RT-PCR analysis of endogenous *S100A4* mRNA expression in Ishikawa cells after treatment with 50 nM rapamycin, 2 μg/ml aphidicolin, or 0.25 μg/ml nocodazole for 24 h. Con control, Nu nuclear, asyn asynchronized, Rap rapamycin, Aph aphidicolin, Noc nocodazole.

with multiplication of values of the two parameters, as described previously [22, 24]. Nuclear immunopositivity for Ki-67 was also counted in at least 1000 cells in five randomly selected fields. Labeling indices (LIs) were then calculated as a percentage.

Statistics

Comparative data were analyzed using the Mann–Whitney *U*-test, and Spearman's correlation coefficient. The cutoff for statistical significance was set as $p < 0.05$.

Results

Regulation of S100A4 expression in Em Ca cells

Since S100A4 is a potent pro-inflammatory regulator [29], we first examined whether S100A4 expression is affected by two inflammation-related cytokines including TNF-α and TGF-β1 in Em Ca cells. The treatment of Ishikawa cells caused an increase in S100A4 expression, along with stabilization of nuclear p65 and/or pSmad2 (Fig. 1a). Transient transfection of the longer *S100A4* promoter constructs revealed that co-transfection of p65, but not Smad2, activated the *S100A4* promoter in a dose-dependent manner, along with increased *S100A4* mRNA expression (Fig. 1b). Analysis of an ~3000 bp of fragment upstream and downstream of the transcription start site in the *S100A4* gene revealed four potential NF-κB/p65 (κB)-binding elements (Fig. 1c). Using a series of 5′-truncated promoters with first intron constructs (Fig. 1c), we found that deletion from −1976 to −447 bp had little effect on induction of promoter activity by p65, and the shortest construct (−447/+1012 bp), which had one putative p65-binding site, was still responsive. By insertion of three nucleotide alterations in the κB-binding site within the shortest construct, the *S100A4* promoter activity in response to p65 was reduced ~20% compared with that of the wild type (Fig. 1d). As shown in Fig. 1e, S100A4 protein expression in both the cytoplasmic and nuclear compartments, as well as the mRNA expression levels (Fig. 1f), were substantially increased in G2/M-arrested cells compared with G1- and early S-arrested cells. These findings suggest that S100A4 is transcriptionally

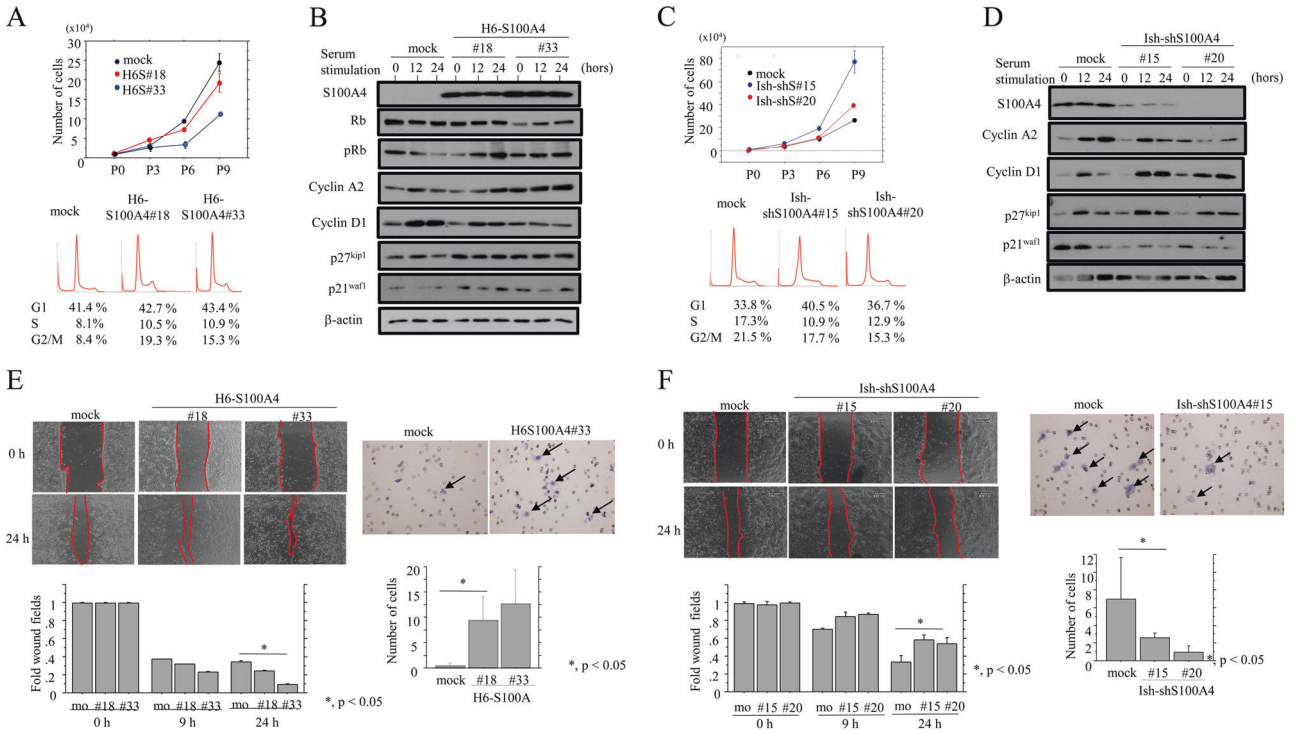

Fig. 2 Relationship of S100A4 expression with cell proliferation and migration in Em Ca cells. a Upper: two independent Hec6 cell lines stably overexpressing S100A4 (H6S#18 and S#33) and empty vector controls, were seeded at low density. The cell numbers are presented as means ± SDs. P0, P3, P6, and P9 are 0, 3, 6, and 9 days after cell passage, respectively. Lower: flow cytometric analysis of the cell cycle analysis for H6-S100A4#18 and #33 cells and control cells at P3. **b** Western blot analysis of the indicated proteins in H6-S100A4 overexpressing cells and controls following re-stimulation of serum-starved (6 h) cells with 10% serum for the indicated times. **c** Upper: two independent Ishikawa cells with knockdown of endogenous S100A4 expression (Ish-shS100A4#15 and #20) and scrambled controls, were seeded at low density. The cell numbers are presented as means ± SDs. P0, P3, P6, and P9 are 0, 3, 6, and 9 days after cell passage, respectively. Lower: cell cycle analysis for Ish-shS100A4#15 and #20 cells and control at P3. **d** Western blot analysis for the indicated proteins in Ish-shS100A4 cells and control cells following re-stimulation of serum-starved (6 h) cells with 10% serum for the indicated times. **e** Left: wound-healing assay with H6-S100A4#18 and #33 cells and mock cells (mo). Phase-contrast images were taken 24 h after making a scratch in the middle of a confluent cell monolayer (upper panel). The values of wound areas were calculated using NIH ImageJ software, with the area at 0 h post-wounding set as 1. The fold wound areas are presented as means ± SDs (lower). Right: migration rate measured using a transwell assay. The H6-S100A4#18 and #33 cells and control cell lines were seeded in a 24-well transwell plate and incubated for 24 h in medium without serum (upper panel). Cells were stained with HE and counted using a light microscope. The cell numbers are presented as means ± SDs (lower panel). **f** Left: wound-healing assay with Ish-shS100A4#15 and #20 cells and mock cells (mo). Phase-contrast images were taken 24 h after making a scratch in the middle of a confluent cell monolayer (upper panel). The values of wound areas were calculated using NIH ImageJ software, with the area at 0 h post-wounding set as 1. The fold wound areas are presented as means ± SDs (lower panel). Right: migration rate measured using a transwell assay. The Ish-shS100A4#15 and #20 and control cells were seeded in a 24-well transwell plate and incubate for 24 h in medium without serum (upper panel). Cells were stained with HE and counted using a light microscope. The cell numbers are presented as means ± SDs (lower panel).

regulated by the NF-κB/p65 pathway and that its expression is altered during cell cycle progression.

Relationship of S100A4 expression with cell proliferation and migration in Em Ca cells

To examine whether S100A4 expression is associated with cell proliferation in Em Ca cells, we established two independent Hec6 cell line clones stably overexpressing S100A4 (H6-S100A4#18 and #33) and two independent Ishikawa cell line clones in which S100A4 expression was blocked by a S100A4-specific shRNA (Ish-shS#15 and Ish-shS#20). The stable Hec6-S100A4 cells showed a tendency towards a low proliferative rate, particularly in the exponential growth phase, along with an increased frequency of cells in the G2/M phase of the cell cycle (Fig. 2a). To further examine alterations in the expression of several cell cycle-related molecules during cell growth, the cell lines were rendered quiescent by serum starvation and were subsequently stimulated with serum. At 12 and 24 h after release into the cell cycle, we observed an increased expression of pRb, cyclin A2, and $p21^{waf1}$ and decreased cyclin D1 expression in Hec6-S100A4 cells relative to the control cells (Fig. 2b). In contrast, Ishikawa-S100A4-knockdown cells proliferated more rapidly and had fewer cells in the S and G2/M phases, along with decreased

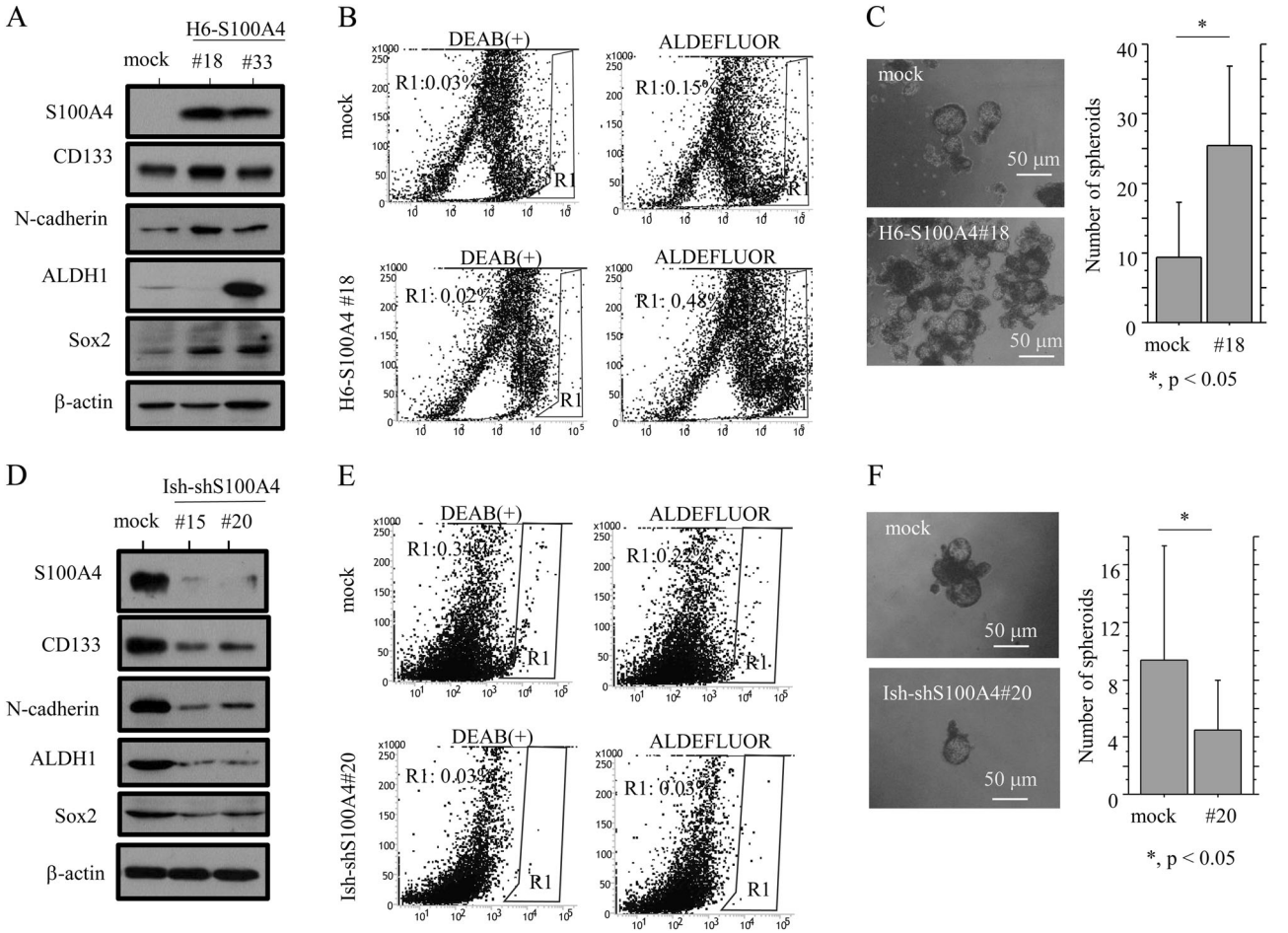

Fig. 3 Relationship between S100A4 expression and CSC properties in Em Ca cells. a Western blot analysis for the indicated proteins in lysates from H6-S100A4#18 and #33 cells and controls. **b** Aldefluor analysis in H6-S100A4#18 cells and controls. **c** Left: phase-contrast photographs of spheroids by H6-S100A4#18 cells and controls following 2 weeks of growth. Right: the numbers of spheroids are presented as means ± SDs. **d** Western blot analysis for the indicated proteins of lysates from Ish-shS100A4#15 and #20 cells and controls. **e** Aldefluor analysis in Ish-shS100A4#20 cells and controls. **f** Left: phase-contrast photographs of spheroids by Ish-shS100A4#20 cells and controls following 2 weeks of growth. Right: the numbers of spheroids are presented as means ± SDs.

expression of cyclin A2 and $p21^{waf1}$ and increased cyclin D1 expression (Fig. 2d).

To examine whether S100A4 contributes to cell migration, we carried out both scratch and migration assays. Hec6-S100A4 cells refilled wounded empty spaces more rapidly, in line with the significantly increased migration rates as compared with the mock cells (Fig. 2e); this was in contrast to the lower values in the Ishikawa-S100A4-knockdown cells (Fig. 2f).

Collectively, these findings suggest that S100A4 expression contributes to modulation of cell proliferation and migration in Em Ca cells.

Relationship between S100A4 expression and CSC properties in Em Ca cells

Since S100A4 is a normal stemness marker [30] we examined the association between S100A4 and CSC properties in Em Ca cells. Hec6-S100A4 cells showed increased expression of several stem cell markers including CD133, N-cadherin, ALDH1, and Sox2 when compared with mock cells (Fig. 3a). The Aldefluor assay also revealed a significant $ALDH1^{high}$ population in the S100A4-overexpressing cells compared with the mock cells (Fig. 3b), in line with the significantly increased number of well-defined, round spheroids that were over 50 μm in diameter (Fig. 3c). In contrast, CSC properties were absent in Ishikawa-S100A4-knockdown cells (Fig. 3d–f). These findings suggest that S100A4 expression is closely associated with induction of CSC properties in Em Ca cells.

S100A4 strongly interacts with NMII in Em Ca cells

S100A4 has no known enzymatic activity and interactions with both intracellular and extracellular proteins are therefore undoubtedly required for its biological functions

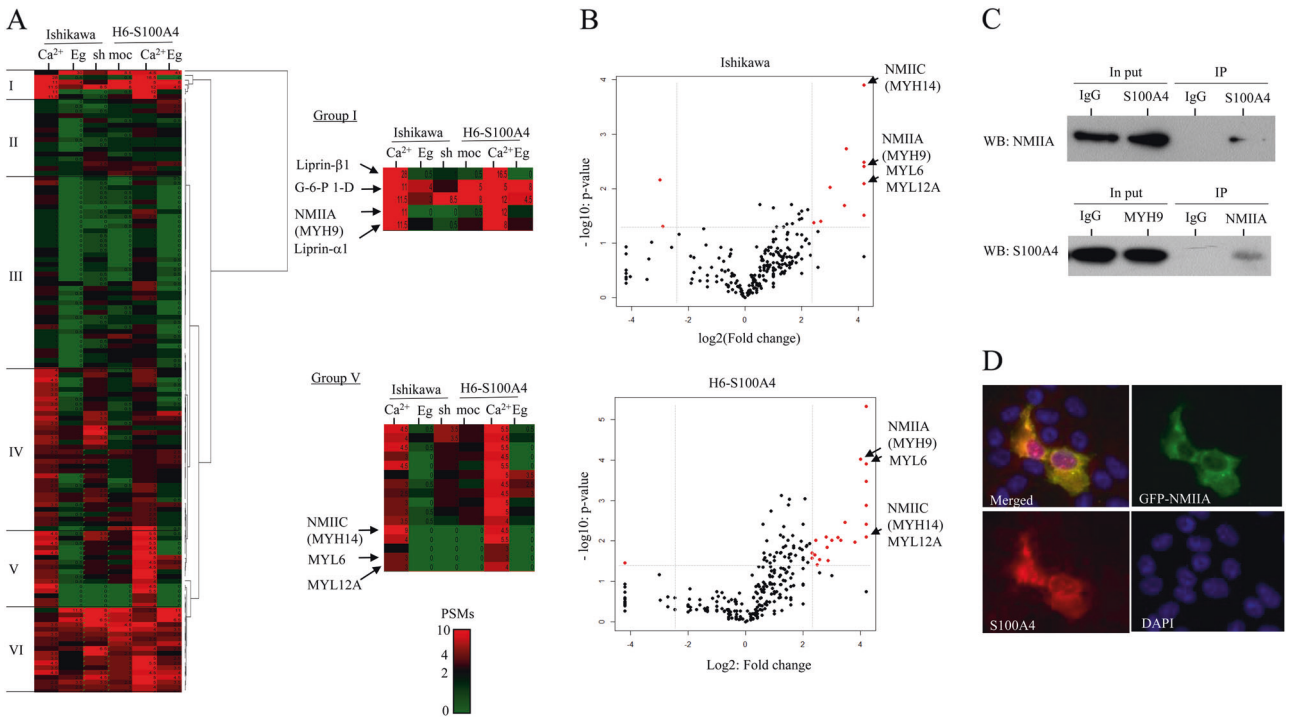

Fig. 4 S100A4 frequently interacts with NMII in Em Ca cells. **a** Unsupervised hierarchical clustering of proteoforms detected by a combination of S100A4-meditaed co-immunoprecipitation and shotgun proteomics assay in Ishikawa cells, Ish-shS100A4 cells, and H6-S100A4 cells in the presence of either 1 mM $CaCl_2$ (Ca^{2+}) or 1 mM EGTA (Eg) or their absence. The values of peptide spectrum matches (PSMs) are color coded as follows; red, black, and green indicated high (>4), neutral [1–4], and low (<1), respectively. Major clusters are shown as groups I to VI. Moc mock cells. **b** Volcano plots generated to compare the relative PSM values obtained from Ca^{2+}-treated relative to EGTA-treated conditions in Ishikawa cells (upper panel) and H6-S100A4 cells (lower panel). Proteoforms with relatively high PSM values are indicated by red-closed dots. **c** Western blotting (WB) with anti-NMIIA (upper panel) and anti-S100A4 antibodies (lower panel) after immunoprecipitation (IP) with the indicated antibodies using Ishikawa cell lysates. Input represents 5% of the total cell extract. Normal rabbit IgG was used as a negative control. **d** After co-transfection of S100A4 and GFP-NMIIA, Ishikawa cells were stained for S100A4. Note the co-localization of the two molecules in cytoplasmic components.

[31, 32]. To identify proteins associated with S100A4, we carried out shotgun proteomics and found a total of 480 and 549 proteoforms in Ishikawa/Ishikawa-S100A4-knockdown cells and Hec6-S100A4 cells, respectively. As shown in Fig. 4a, hierachical clustering revealed that these proteins could be readily categorized into six groups. Of these, groups I and V demonstrated high peptide spectrum matches (PSM) with the proteoforms detected in the Ca^{2+}-treated categories; this was in contrast to the low values in EGTA-treated categories in both Ishikawa and Hec6 cells (Supplementary Table S2). We also created a volcano plot, which represents each proteoform as a relative PSM calculated as the log2 fold-change in Ca^{2+}-relative to EGTA-categories and the statistical confidence (in $-\log10\ p$ value). A total of 11 and 21 proteoforms identified to the right were outliers in Ishikawa and Hec6 cells, respectively (Fig. 4b and Supplementary Table S3). Based on the above data, we focused on NMII heavy chains including NMIIA (MYH9) and NMIIC (MYH14), which were strongly enriched in S100A4 co-immunoprecipitates. Furthermore, the association of S100A4 with NMIIA was confirmed by immunoprecipitation-western blot analysis (Fig. 4c) and dual immunofluorescence staining (Fig. 4d).

Relationship between NMII and EMT/CSC properties in Em Ca cells

Since the biological activity of S100A4 depends on interactions with its potential binding partners [31, 32], we evaluated the function of NMII in Em Ca cells using blebbistatin, a synthetic chemical compound that effectively and reversibly blocks the ATPase activity of NMII, without inhibiting class I, V, and X myosin superfamily members [33]. The treatment of Hec6, but not Ishikawa, cells with blebbistatin resulted in a dramatically altered morphology toward a fibroblastic appearance (Fig. 5a), while there was a significant increase in the number of senescence-like and SA-β-gal positive cells in both cell types (Fig. 5b, c). The treatment also caused a significant decrease in cell growth rates (Fig. 5d), along with an increase in the proportion of cells in the G2/M phases (Fig. 5e), significant alterations in the expression of pRb and $p21^{waf1}$ (Fig. 5f), and a significant increase in migration capacity (Fig. 5g) in both

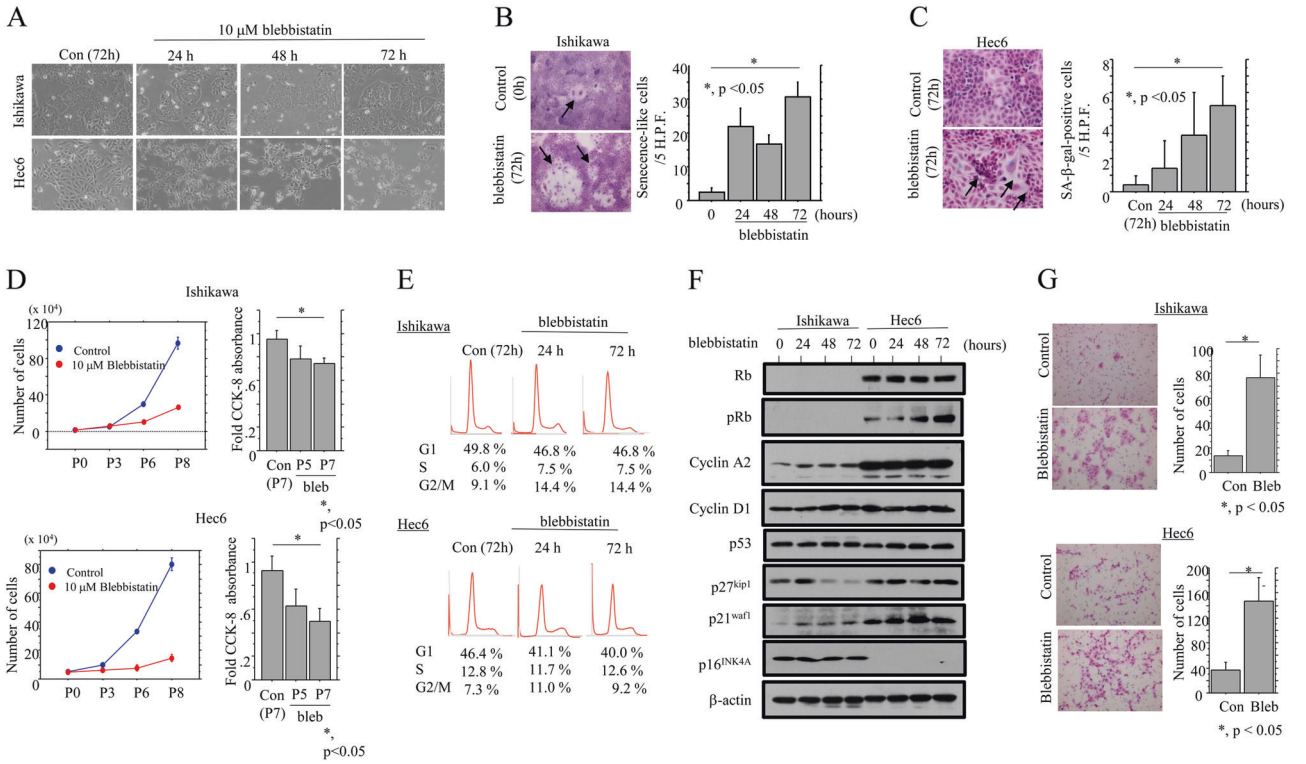

Fig. 5 Inhibition of NMII by blebbistatin alters cell morphology, proliferation, and migration in Em Ca cells. a Phase-contrast image of Ishikawa and Hec6 cells for the time shown following treatment with 10 μM blebbistatin. Note the switch towards a fibroblast-like morphology in Hec6, but not Ishikawa, cells. Con control. **b** Left: Ishikawa cells with senescence-like features (indicated by arrows) after treatment with 10 μM blebbistatin for 72 h. Original magnification, ×100. Right: number of senescence-like cells per five high-power field (HPF). **c** Left: SA-β-gal positive Hec6 cells (indicated by arrows) after treatment with 10 μM blebbistatin for 72 h. Original magnification, ×100. Right: number of SA-β-gal positive cells per five high-power fields (HPF). **d** Left: Ishikawa (upper) and Hec6 cells (lower) were seeded at low density with or without 10 μM blebbistatin. Cell numbers are presented as means ± SDs. P0, P3, P6, and P8 are 0, 3, 6, and 8 days after cell passage, respectively. Right: Ishikawa and Hec6 cells were seeded at 1×10^3 cells in 96-well plates with or without 10 μM blebbistatin (bleb) for the times shown. Viable cell numbers were quantitated using a Cell Counting Kit-8 (CCK-8). Absorbance values are presented as means ± SDs. P5 and P7 indicate 5 and 7 days after blebbistatin treatment, respectively. This experiment was performed in triplicate using independent samples. Con control. **e** Flow cytometric cell cycle analysis for Ishikawa (upper) and Hec6 cells (lower) after 10 μM blebbistatin treatment for the times shown. **f** Western blot analysis of the indicated proteins in Ishikawa and Hec6 cell lysates after 10 μM blebbistatin treatment for the times shown. **g** Migration rate measured using a transwell assay. Ishikawa (upper) and Hec6 cells (lower) were seeded in a 24-well transwell plates and incubated in medium without serum after 10 μM blebbistatin treatment for 24 h. Cells were stained by HE and counted using a light microscope. The cell numbers are presented as means ± SDs.

cells. Finally, the Aldefluor assay revealed that blebbistatin increased the ALDH1^{high} population (Fig. 6a); these observations were consistent with the increased expression of several EMT/CSC markers including vimentin, pSmad2, Slug, ZEB1, Twist1, and ALDH1 in Hec6, but not Ishikawa, cells (Fig. 6b). Taken together, these findings suggest that suppression of NMII function by blebbistatin also affects EMT/CSC properties and the proliferation rate of Em Ca cells, and are consistent with the results we obtained with Hec6 cells that overexpress S100A4.

TCGA data analysis in UCS

Since the *MYH9* gene is frequently altered in human invasive lobular carcinoma and the aberration results in altered gene expression [34], we also examined the relationship between genetic alterations and mRNA expression for the *S100A4* and *MYH9* genes in UCS using the data from TCGA. The *S100A4* and *MYH9* gene abnormities including gene mutations and copy-number alterations were observed in 77 and 88%, respectively, in the 56 TCGA-UCS cases (Supplementary Fig. S2A). *S100A4* mRNA expression was significantly higher in UCS cases with gene amplification as compared with those with shallow deletions (Supplementary Fig. S2B). In contrast, the associations for *MYH9* gene were not evaluated, since the data for MYH9 mRNA expression could not be obtained from the UCS-TCGA database.

IHC findings in UCS

Representative IHC findings for S100A4 and functionally related molecules in UCS are illustrated in Fig. 7a. Nuclear/

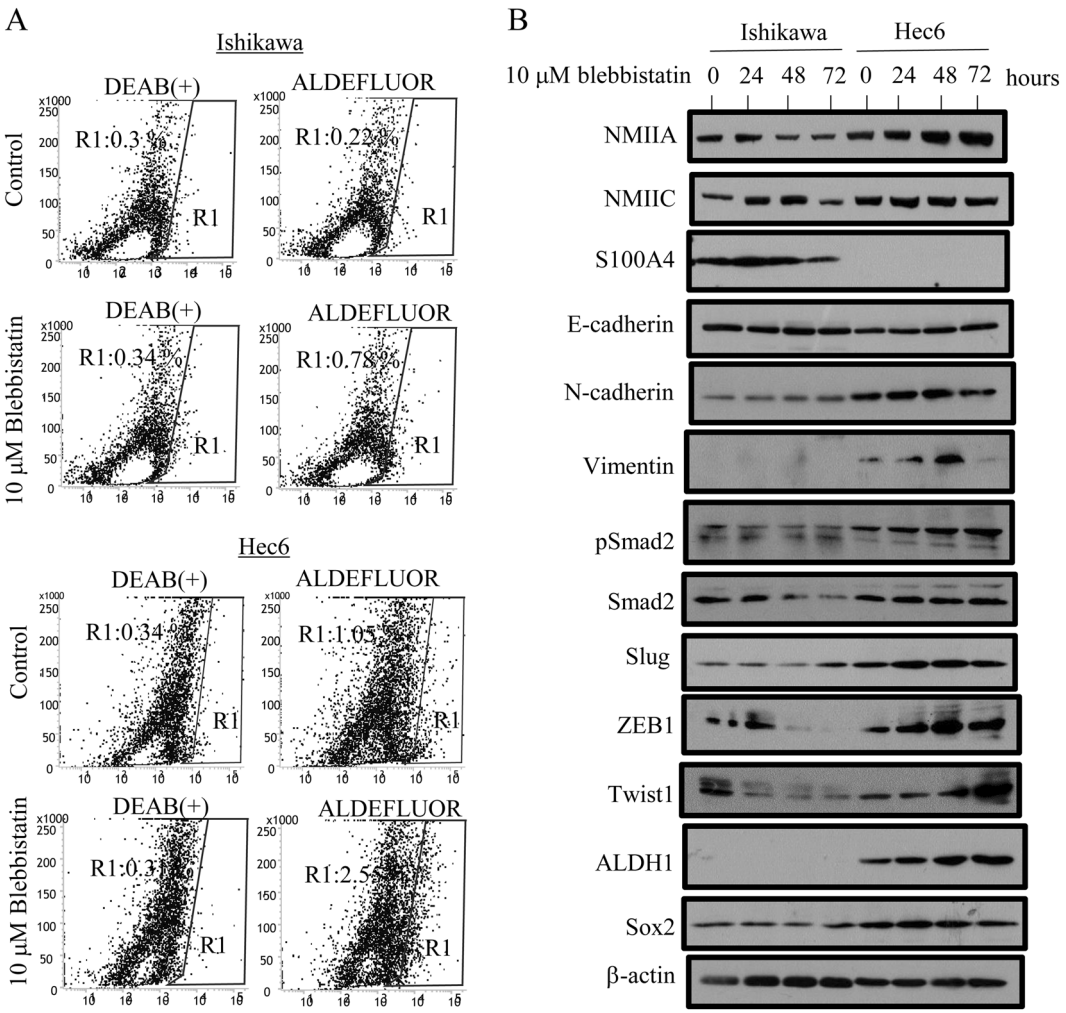

Fig. 6 Inhibition of NMII by blebbistatin enhances CSC properties in Em Ca cells. a Aldefluor analysis in Ishikawa (upper) and Hec6 cells (lower) after 10 μM blebbistatin treatment for 24 h. **b** Western blot analysis for the indicated proteins in Ishikawa and Hec6 cell lysates after treatment with 10 μM blebbistatin for the indicated times.

cytoplasmic immunostaining for S100A4 and ALDH1, cytoplasmic immunoreaction for NMIIA and vimentin, and nuclear or membrane stainings for pp65, Sox2, Slug, Ki-67, and E-cadherin were observed in both carcinomatous and sarcomatous elements of UCS. Average IHC scores for S100A4, ALDH1, Slug, and vimentin were significantly higher in sarcomatous components than those of carcinomatous elements. Conversely, significantly higher E-cadherin scores and Ki-67 LIs were obtained in the latter. There was no significant difference in NMIIA and pp65 scores between the two components (Fig. 7b).

As shown in Table 2, the average S100A4 score was positively correlated with ALDH1, Slug, and vimentin scores, and inversely with Ki-67 LIs in UCS. There were also positive correlations between vimentin, Slug, and ALDH1 scores, while none of the markers were associated with NMIIA and pp65 status. In addition, S100A4 score also positively correlated with ALDH1, pp65, and vimentin scores and negatively with Ki-67 LIs in carcinomatous and sarcomatous components, respectively (Supplementary Table S4).

Discussion

Several observations in the present study clearly demonstrate that S100A4 expression is under the transcriptional control of TNF-α/p65, but not TGF-β1/Smad2, signaling in Em Ca cells. First, the treatment of Ishikawa cells with both TNF-α and TGF-β1 caused an increase in S100A4 expression, along with stabilization of pSmad2 and/or nuclear p65. Second, the transfection of p65 resulted in upregulation of *S100A4* mRNA. Third, the overexpression of p65, but not Smad2, enhanced *S100A4* promoter activity in Em Ca cells, although mutations in the putative κB-binding site in the first intron had minor effects on p65-responsiveness. Since

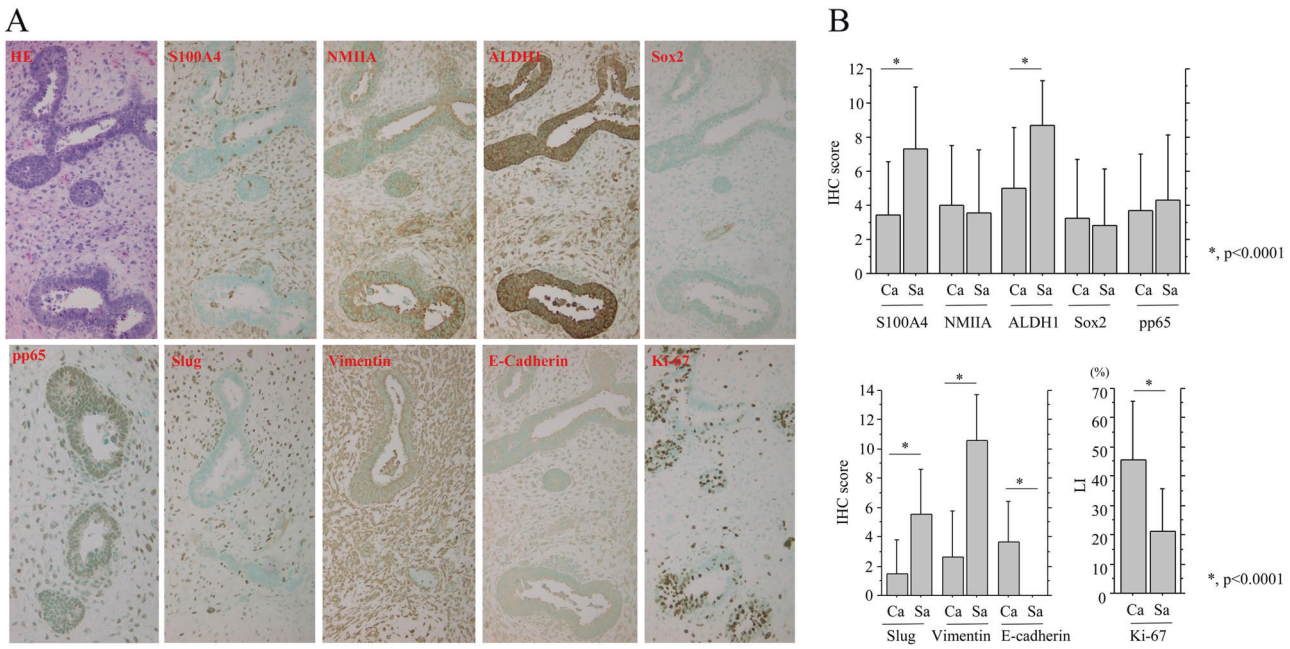

Fig. 7 IHC findings in serial sections of UCS tissues. a HE and IHC staining for the indicated proteins in UCS. Original magnification, ×100. **b** IHC score for the indicated molecules in carcinomatous and sarcomatous categories.

Table 2 Correlations between S100A4 and related IHC markers in uterine carcinosarcomas.

	S100A4 ρ(p)	NMIIA ρ(p)	ALDH1 ρ(p)	Sox2 ρ(p)	pp65 ρ(p)	Slug ρ(p)	Vimentin ρ(p)	E-cadherin ρ(p)
NMIIA	0.18 (0.13)	*	*	*	*	*	*	*
ALDH1	0.58 (<0.0001)	0.16 (0.17)	*	*	*	*	*	*
Sox2	−0.2 (0.1)	0.19 (0.11)	−0.01 (0.9)	*	*	*	*	*
pp65	0.16 (0.2)	0.2 (0.1)	0.2 (0.09)	0.05 (0.7)	*	*	*	*
Slug	0.43 (0.0004)	0.01 (0.8)	0.43 (0.0003)	−0.01 (0.9)	0.01 (0.9)	*	*	*
Vimentin	0.46 (0.0002)	−0.08 (0.5)	0.44 (0.0002)	0.02 (0.8)	0.02 (0.9)	0.6 (<0.0001)	*	*
E-cadherin	−0.15 (0.2)	0.3 (0.03)	−0.16 (0.19)	0.11 (0.36)	0.16 (0.17)	−0.15 (0.2)	−0.4 (0.001)	*
Ki-67	−0.48 (<0.0001)	−0.02 (0.05)	−0.22 (0.07)	0.2 (0.09)	−0.03 (0.8)	−0.3 (0.014)	−0.4 (0.002)	0.51 (<0.0001)

ρ Spearman's correlation coefficient, *IHC* immunohistochemistry

*Not examined

there was no correlation between S100A4 and pp65 IHC status in UCS, we infer that the mechanism by which p65 drives transcriptional activation S*100A4* is complex. In fact, it has been reported that a κ recognition component (KRC) binding κB-like element co-operates with factors binding minisatellite DNA sequences, thereby acting as an intronic enhancer of *S100A4* [35]. Since we observed increased TGF-β1-dependent S100A4 expression via stabilization of nuclear p65, we suggest there may be crosstalk between the TGF-β and NF-κB signaling pathways, since TGF-β-induced TGF-β-kinase 1 enhances NF-κB activation [36].

We also found that Hec6-S100A4 overexpressing cells had a reduced proliferative rate and enhanced migration capability, along with increases in both G2/M fraction and expression of pRb, cyclin A2, and $p21^{waf1}$, while the opposite was observed in the Ishikawa-S100A4-knockdown cells. Given the findings of increased *S100A4* mRNA and protein expression in G2/M phase, it is possible that S100A4 may be a positive activator of cell cycle inhibitors, particularly at the G2/M checkpoint. This would be in line with our IHC findings of an inverse correlation between S100A4 score and Ki-67 LI values in UCS tissues. Interestingly, S100A4 may be involved in guiding cyclin B1 to spindle pole areas prior to cyclin B1-Cdk1 activation [37]. Experiments have also revealed that migratory cells have a lower proliferation rate in comparison with cells in the tumor core, which indicates an inverse correlation between cell proliferation and mobility [38–40].

In our results, a combination of co-immunoprecipitation and shotgun proteomics revealed that S100A4 strongly

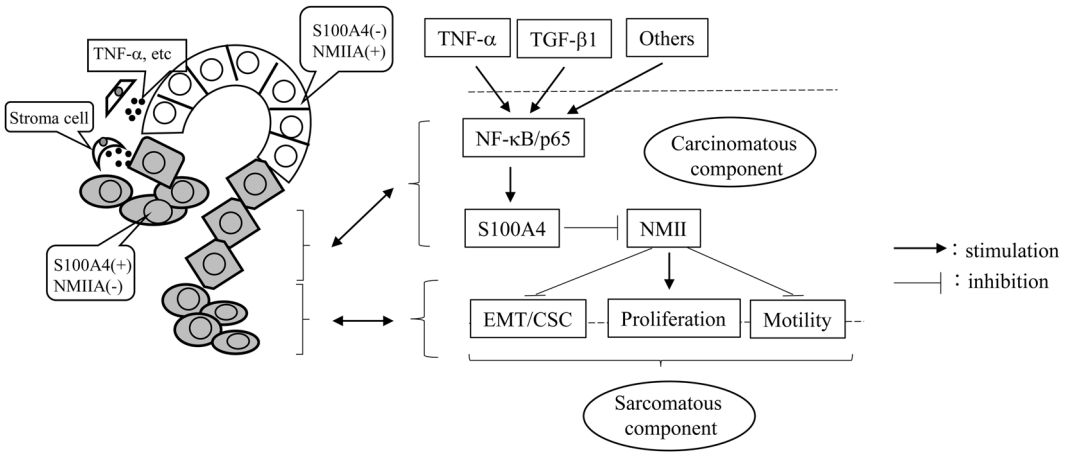

Fig. 8 Schematic representation of the role of an S100A4/NMII-driven signaling cascade as progenitor for divergent sarcomatous differentiation in UCS. Association of the cascade engenders EMT/CSC properties, as well as changes in cell proliferation and migration capability.

bound to NMII components including MYH9 and MYH14. Moreover, the inhibition of NMII by blebbistatin, which is likely to affect specific NMII functions [33], phenocopied the results we obtained in the Hec6 cells overexpressing S100A4, supporting the idea that S100A4 could be an effective inhibitor of NMII polymerization [17, 41–43].

Importantly, the overexpression of S100A4 was closely associated with the induction of CSC properties, including an increased expression of several stemness markers, enhancement of sphere-forming capability, and an increased ALDH1^{high} population in Em Ca cells. In contrast, stemness features were completely absent in the S100A4-knockdown cells. Our results are consistent with those of others, who have demonstrated that S100A4 directly contributes to the self-renewal and survival of gliomas and head and neck cancers [19, 44].

In addition to the effects on cell proliferation and migration, Hec6 cells (but not Ishikawa cells) treated with blebbistatin also showed an alteration in cell morphology toward EMT-like appearances and induction of several CSC features, although the effects for increased numbers of senescence-associated cells, probably due to cell cycle arrest at G2/M phase, were observed in both cell lines. Given the notion that EMT is associated with acquisition of stemness in a variety of human malignancies [15], we suggest that S100A4-mediated inhibition of NMII activity may play an important role in the establishment and maintenance of EMT/CSC properties in UCS, resulting in the development of mesenchymal cell morphology. This conclusion is supported by our IHC experiments that revealed positive correlations between S100A4 with ALDH1, vimentin, and Slug scores, which in turn were closely linked to EMT/CSC features, particularly in the sarcomatous components of UCS. With regard to our findings showing relatively minor changes in EMT/CSC features in Ishikawa cells treated with blebbistatin as compared with Hec6 cells, it appears that S100A4 may require some cell type-specific factors in order to inhibit NMII function. Further studies will be required in order to elucidate these factors.

Conclusion

Together, our results suggest a novel functional role of S100A4/NMII-related signaling in UCS (Fig. 8). S100A4 is transcriptionally upregulated through TNF-α- and/or TGF-β1-mediated activation of NF-κB signaling, as well as other factors. By inhibiting NMII function, the overexpression of S100A4 induces EMT/CSC properties and changes in cell proliferation and migration capability, which in turn results in divergent sarcomatous differentiation from carcinomatous components in UCS.

Acknowledgements We thank Dr Robert Adelstein for the generous gift of the CMV-GFP-NMHC II-A plasmid used in this study. This study was supported by a grant from JSPS KAKENHI Grant Number 17K08703.

Author contributions MT and MS carried out the majority of the experiments, analyzed the data, and wrote the manuscript. They were helped by MH, YO, and AY. RK, MT, and YK were involved in the study design and data collection. All authors reviewed and approved the final manuscript.

Compliance with ethical standards

Conflict of interest The authors declare that they have no conflict of interest.

Publisher's note Springer Nature remains neutral with regard to jurisdictional claims in published maps and institutional affiliations.

References

1. McCluggage WG. Malignant biphasic uterine tumours: carcinosarcomas or metaplastic carcinomas? J Clin Pathol. 2002;55:321–5.
2. McCluggage WG. Uterine carcinosarcomas (malignant mixed mullerian tumors) are metaplastic carcinomas. Int J Gynecol Cancer. 2002;12:687–90.
3. D'Angelo E, Prat J. Uterine sarcomas: a review. Gynecol Oncol. 2010;23:694–702.
4. Thompson L, Chang B, Barsky SH. Monoclonal origins of malignant mixed tumors (carcinosarcoma). Evidence for a divergent histogenesis. Am J Surg Pathol. 1996;20:277–85.
5. Gupta GP, Massague J. Cancer metastasis: building a framework. Cell. 2006;127:679–95.
6. Casas E, Kim J, Bendesky A, Ohno-Machado L, Wolfe CJ, Yang J. Snail2 is an essential mediator of twist-induced epithelial mesenchymal transition and metastasis. Cancer Res. 2011;71:245–54.
7. Savagner P, Yamada KM, Thiery JP. The zinc-finger protein slug causes desmosome dissociation, an initial and necessary step for growth factor-induced epithelial-mesenchymal transition. J Cell Biol. 1997;137:1403–19.
8. Batlle E, Sancho E, Franci C, Dominguez D, Monfar M, Baulida J. et al. The transcription factor snail is a repressor of E-cadherin gene expression in epithelial tumour cells. Nat Cell Biol. 2000;2:84–9.
9. Bolos V, Peinado H, Perez-Moreno MA, Fraga MF, Esteller M, Cano A. The transcription factor Slug represses E-cadherin expression and induces epithelial to mesenchymal transitions: a comparison with Snail and E47 repressors. J Cell Sci. 2003;116:499–511.
10. Li J, Zhou BP. Activation of β-catenin and Akt pathways by Twist are critical for the maintenance of EMT associated cancer stem cell like characters. BMC Cancer. 2011;11:49.
11. Thiery JP. Epithelial-mesenchymal transitions in tumour progression. Nat Rev Cancer. 2002;2:442–54.
12. Sarrio D, Rodriguez-Pinilla SM, Hardisson D, Cano A, Moerno-Bueno G, Palacios J. Epithelial-mesenchymal transition in breast cancer relates to the basal-like phenotype. Cancer Res. 2006;68:989–97.
13. Castilla MA, Moreno-Bueno G, Romero-Perez L, Van De Vijver K, Biscuola M, Lopez-Garcia MA, et al. Micro-RNA signature of the epithelial-mesenchymal transition in endometrial carcinosarcoma. J Pathol. 2011;223:72–80.
14. Reya T, Morrison SJ, Clarke MF, Weissman IL. Stem cells, cancer, and cancer stem cells. Nature. 2001;414:105–11.
15. Mani SA, Guo W, Liao MJ, Eaton EN, Ayyanan A, Zhou AY, et al. The epithelial-mesenchymal transition generates cells with properties of stem cells. Cell. 2008;133:704–15.
16. Griorian M, Andresen S, Tulchinsky E, Kriajevska M, Carlberg C, Kruse C, et al. Tumor suppressor p53 protein is a new target for the metastasis-associated Mts1/S100A4 protein: functional consequences of their interaction. J Biol Chem. 2001;276:22699–708.
17. Li Z-H, Bresnick AR. The S100A4 metastasis factor regulates cellular motility via a direct interaction with myosin-IIA. Cancer Res. 2006;66:5173–80.
18. Semov A, Moreno MJ, Onichtchenko A, Abulrob A, Ball M, Ekiel I, et al. Metastasis-associated protein S100A4 induces angiogenesis through interaction with Annexin II and accelerated plasmin formation. J Biol Chem. 2005;280:20833–41.
19. Chow K-H, Park HJ, George J, Yamamoto K, Gallup AD, Graber JH, et al. S100A4 is a biomarker and regulator of glioma stem cells that is critical for mesenchymal transition in glioblastoma. Cancer Res. 2017;77:5360–73.
20. Akiya M, Yamazaki M, Matsumoto T, Kawashima Y, Oguri Y, Kajita S, et al. Identification of LEFTY as a molecular marker for ovarian clear cell carcinoma. Oncotarget. 2017;8:63646–64.
21. Saegusa M, Hashimura M, Kuwata T, Hamano M, Okayasu I. Crosstalk between NF-κB/p65 and β-catenin/TCF4/p300 signalling pathways through alterations in GSK-3β expression during transdifferentiation of endometrial carcinoma cells. J Pathol. 2007;213:35–45.
22. Inoue H, Takahashi H, Hashimura M, Eshima K, Akiya M, Matsumoto T et al. Cooperation of Sox4 with β-catenin/p300 complex in transcriptional regulation of the *Slug* gene during divergent sarcomatous differentiation in uterine carcinosarcoma. BMC Cancer. 2016;16:53.
23. Saegusa M, Hashimura M, Kuwata T. Sox4 functions as a positive regulator of β-catenin signaling through upregulation of *TCF4* during morular differentiation of endometrial carcinomas. Lab Invest. 2012;92:511–21.
24. Inoue H, Hashimura M, Akiya M, Chiba R, Saegusa M. Functional role of ALK-related signal cascades on modulation of epithelial-mesenchymal transition and apoptosis in uterine carcinosarcoma. Mol Cancer. 2017;16:37.
25. Saegusa M, Hashimura M, Kuwata T, Hamano M, Okayasu I. β-Catenin simultaneously induces activation of the p53-p21WAF1 pathway and overexpression of cyclin D1 during squamous differentiation of endometrial carcinoma cells. Am J Pathol. 2004;164:1739–49.
26. Kawashima Y, Takahashi N, Satoh M, Saito T, Kado S, Nomura F et al. Enhanced recovery of lyophilized peptides in shotgun proteomics by using an LC-ESI-MC compatible surfactant. Proteomics. 2013;13:751–5.
27. Kawashima Y, Kodera Y, Singh A, Matsumoto M, Matsumoto H. Efficient extraction of proteins from formalin-fixed paraffin-embedded tissues requires higher concentration of tris(hydroxymethyl)aminomethane. Clin Proteomics. 2014;11:4.
28. Zaino R, Carinelli SG, Ellenson LH, Eng C, Katabuchi H, Konishi I, et al. Tumours of the uterine corpus. In: Kurman RJ, Carcangiu ML, Herrington CS, Young RH, editors. WHO classification of tumours of female reproductive organs. Lyon: IARC; 2014. p. 121–54.
29. Fei F, Qu J, Li C, Wang X, Li Y, Zhang S. Role of metastasis-induced protein S100A4 in human non-tumor pathophysiologies. Cell Biosci. 2017;7:64.
30. Mazzucchelli L. Protein S100A4: too long overlooked by pathologists? Am J Pathol. 2002;160:7–13.
31. Helfman DM, Kim EJ, Lukanidin E, Grigorian M. The metastasis associated protein A100A4: role of tumour progression and metastasis. Br J Cancer. 2005;92:1955–8.
32. Boye K, Malandsmo GM. S100A4 and metastasis: a small actor playing many roles. Am J Pathol. 2010;176:528–35.
33. Straight AF, Cheung A, Limouze J, Chen I, Westwood NJ, Sellers JR, et al. Dissecting temporal and spatial control of cytokinesis with a myosin II inhibitor. Science. 2003;299:1743–7.
34. Kas SM, de Ruiter JR, Schipper K, Annunziato S, Schut E, Klarenbeek S, et al. Insertional mutagenesis identifies drivers of a novel oncogenic pathway in invasive lobular breast carcinoma. Nat Genet. 2017;49:1219–30.
35. Cohn MA, Hjeimso I, Wu L-C, Guldberg P, Lukanidin EM, Tulchinsky EM. Characterization of Sp1, AP-1, CBF and KRC binding sites and minisatellite DNA as functional elements of the metastasis-associated *mts1/S100A4* gene intronic enhancer. Nucleic Acids Res. 2001;29:3335–46.
36. Freudlsperger C, Bian Y, Wise SC, Burnett J, Coupar J, Yang X et al. Van Waes C. TGF-β and NF-κB signal pathway cross-talk is mediated through TAK1 and SMAD7 in a subset of head and neck cancers. Oncogene. 2013;32:1549–59.

37. Egeland EV, Boye K, Pettersen SJ, Haugen MH, Oyjord T, Malerod L et al. Enrichment of nuclear S100A4 during G2/M in colorectal cancer cells: possible association with cyclin B1 and centrosomes. Clin Exp Metastasis. 2015;32:755–67.
38. Giese A, Loo MA, Tran N, Haskett D, Coons SW, Berens ME. Dichotomy of astrocytoma migration and proliferation. Int J Cancer. 1996;67:275–82.
39. Giese A, Bjerkvig R, Berens ME, Westphal M. Cost of migration: invasion of malignant glioma and implications for treatment. J Clin Oncol. 2003;21:1624–36.
40. Merzak A, McCrea S, Koocheckpour S, Pilkington GJ. Control of human glioma cell growth, migration and invasion in vitro by transforming growth factor beta 1. Br J Cancer. 1994;70: 199–203.
41. Kriajevska M, Tarabykina S, Bronstein I, Maitland N, Lomonosov M, Hansen K et al. Metastasis-associated Mts1 (S100A$) protein modulates protein kinase C phosphorylation of the heavy chain of nonmuscle myosin. J Biol Chem. 1998;273:9852–6.
42. Li Z-H, Spektor A, Varlamova O, Bresnick AR. Mts1 regulates the assemble of nonmuscle myosin-IIA. Biochemistry. 2003;42: 14258–66.
43. Pecci A, Ma X, Savoia A, Adelstein RS. MYH9: structure, functions and role of non-muscle myosin IIA in human disease. Gene. 2018;664:152–67.
44. Lo J-F, Yu C-C, Chiou S-H, Huang C-Y, Jan C-I, Lin S-C et al. The epithelial-mesenchymal transition mediator S100A4 maintains cancer-initiating cells in head and neck cancers. Cancer Res. 2011;71:1912–23.